

Sensitivity study of forecasted aftershock seismicity based on Coulomb stress calculation and rate- and state-dependent frictional response

Journal Article**Author(s):**

Cocco, M.; Hainzl, S.; Catalli, F.; Enescu, B.; Lombardi, A. M.; Woessner, J.

Publication date:

2010-05

Permanent link:

<https://doi.org/https://doi.org/10.3929/ethz-c-000018638>

Rights / license:

[In Copyright - Non-Commercial Use Permitted](#)

Originally published in:

Journal of Geophysical Research: Solid Earth 115, <https://doi.org/10.1029/2009JB006838>



Sensitivity study of forecasted aftershock seismicity based on Coulomb stress calculation and rate- and state-dependent frictional response

M. Cocco,¹ S. Hainzl,² F. Catalli,¹ B. Enescu,^{2,3} A. M. Lombardi,¹ and J. Woessner⁴

Received 3 August 2009; accepted 18 November 2009; published 27 May 2010.

[1] We use the Dieterich (1994) physics-based approach to simulate the spatiotemporal evolution of seismicity caused by stress changes applied to an infinite population of nucleating patches modeled through a rate- and state-dependent friction law. According to this model, seismicity rate changes depend on the amplitude of stress perturbation, the physical constitutive properties of faults (represented by the parameter $A\sigma$), the stressing rate, and the background seismicity rate of the study area. In order to apply this model in a predictive manner, we need to understand the impact of physical model parameters and the correlations between them. First, we discuss different definitions of the reference seismicity rate and show their impact on the computed rate of earthquake production for the 1992 Landers earthquake sequence as a case study. Furthermore, we demonstrate that all model parameters are strongly correlated for physical and statistical reasons. We discuss this correlation, emphasizing that the estimations of the background seismicity rate, stressing rate, and $A\sigma$ are strongly correlated to reproduce the observed aftershock productivity. Our analytically derived relation demonstrates the impact of these model parameters on the Omori-like aftershock decay: the c value and the productivity of the Omori law, implying a p value smaller than or equal to 1. Finally, we discuss an optimal strategy to constrain model parameters for near-real-time forecasts.

Citation: Cocco, M., S. Hainzl, F. Catalli, B. Enescu, A. M. Lombardi, and J. Woessner (2010), Sensitivity study of forecasted aftershock seismicity based on Coulomb stress calculation and rate- and state-dependent frictional response, *J. Geophys. Res.*, 115, B05307, doi:10.1029/2009JB006838.

1. Introduction

[2] The spatial evolution of seismicity is commonly modeled in terms of coseismic and postseismic stress changes. Stress perturbations are simulated to model fault interaction and earthquake triggering [Harris, 1998; King and Cocco, 2001; Freed, 2005; Steacy *et al.*, 2005a, and references therein]. Several articles have pointed out the correlation between Coulomb stress changes and the seismicity rate changes after moderate- to large-magnitude earthquakes [Stein, 1999; Toda and Stein, 2003]. However, these studies show that, in order to model the spatial and temporal evolution of seismicity, the fault constitutive properties have to be taken into account. To this task Dieterich [1992, 1994] proposed a model to simulate the changes in the rate of earthquake production caused by

stress changes applied to an infinite population on nucleating patches modeled through a rate- and state-dependent friction law. This model has been discussed by a theoretical point of view [see Gomberg *et al.*, 2005a, and references therein] and widely applied to different tectonic areas [e.g., Toda *et al.*, 1998, 2005; Dieterich *et al.*, 2000; Gross, 2001; Toda and Stein, 2003; Catalli *et al.*, 2008; Llenos *et al.*, 2009].

[3] According to the Dieterich model, seismicity rate changes depend on the amplitude of the stress perturbation, the physical constitutive properties of faults represented by the parameter $A\sigma$ (where A is the constitutive parameter controlling the direct effect of friction in the rate and state formulation and σ is the effective normal stress), the stressing rate, as well as by the background seismicity rate of the study area.

[4] The Dieterich [1994] model has been proposed as a reliable physics-based approach to forecast seismicity rate changes and to compute earthquake probability changes [Toda and Stein, 2003; Toda *et al.*, 2005]. It has also been proposed as the key ingredient of approaches aimed at evaluating the change in probability of occurrence of a large earthquake on a specific fault caused by the coseismic stress changes generated by previous earthquakes occurred nearby [Stein *et al.*, 1997; Parsons *et al.*, 2000]. This latter issue is

¹Istituto Nazionale di Geofisica e Vulcanologia (INGV), Rome, Italy.

²Helmholtz Centre Potsdam, GFZ German Research Centre for Geosciences, Potsdam, Germany.

³Also at National Research Institute for Earth Science and Disaster Prevention (NIED), Tsukuba, Japan.

⁴Swiss Seismological Service, ETH Zurich, Zurich, Switzerland.

still controversially debated within the scientific community, since different opinions exist concerning the actual capability of evaluating the changes in single-fault earthquake probability through a model assuming an infinite population of nucleation patches [see *Hardebeck, 2004; Gombert et al., 2005b*].

[5] In the present article we only mention the problem of computing aftershock probability through seismicity rate changes, because our focus is on computing seismicity rate changes caused by coseismic stress perturbations. We do not discuss here the problem of the reliable assessment of time-dependent earthquake probabilities for main shocks through renewal approaches. Our main goal is to discuss the ability to forecast seismicity rate changes through a physics-based model, in order to assess its relevance for society.

[6] This article presents the results of research activities matured in the framework of two projects, namely Network of Research Infrastructures for European Seismology (NERIES, <http://www.neries-eu.org>) and Seismic Early Warning for Europe (SAFER, <http://www.saferproject.net>), funded by European Community within the sixth framework program. We have faced the challenging task to perform a retrospective testing experiment to forecast aftershocks patterns using the 1992 Landers earthquake as a case study. While *Hainzl et al. [2009]* have studied the problem of aftershock modeling, taking into account the variability caused by uncertainties of computed stress perturbations, the goal of the present manuscript is to understand the role of the main physical input parameters in forecasting seismicity rate changes through the Dieterich's physics-based model. This sensitivity study is particularly important in order to perform a retrospective validation, which requires an accurate analysis of the variability and the estimate of best model parameters. The result of a retrospective test of stress-based models in comparison to purely statistical models is presented in the follow-up article by J. Woessner et al. (A retrospective comparative test for the 1992 Landers sequence, submitted to *Journal of Geophysical Research*, 2009) for the 1992 Landers earthquake sequence.

2. Methodology

[7] In this section we summarize the methodologies commonly adopted to compute Coulomb stress changes and to forecast seismicity rate changes through the Dieterich's model. The main goal is to point out the most important physical parameters that have to be constrained in order to perform robust applications to real study cases taking into account the correlation between the model parameters.

2.1. Computing Coulomb Stress Changes

[8] Coulomb stress changes (ΔCFF) are calculated through the following relation:

$$\Delta\text{CFF} = \Delta\tau + \mu \times (\Delta\sigma_n + \Delta P), \quad (1)$$

where $\Delta\tau$ is the shear stress in the direction of slip on the assumed causative fault plane, $\Delta\sigma_n$ is the normal stress changes (positive for unclamping or extension), μ is the friction coefficient, and ΔP is the pore pressure change [see *Harris, 1998; King and Cocco, 2001*]. The relation used to

compute the coseismic pore pressure changes distinguishes the constant apparent friction model from the isotropic poroelastic model [*Cocco and Rice, 2002*]. According to the former model, pore pressure changes depend on the normal stress changes $\Delta P = -B\Delta\sigma_n$, where B is the Skempton coefficient which varies between 0 and 1 [*Beeler et al., 2000; Cocco and Rice, 2002*, and references therein]. Therefore, using this model, equation (1) can be written as

$$\Delta\text{CFF} = \Delta\tau + \mu' \Delta\sigma_n, \quad (2)$$

where $\mu' = \mu(1 - B)$ is usually called the effective friction coefficient. On the contrary, the isotropic poroelastic model assumes that pore pressure changes depend on the volumetric stress changes (first invariant of the stress perturbation tensor) $\Delta P = -B(\Delta\sigma_{kk}/3)$, and therefore equation (1) becomes

$$\Delta\text{CFF} = \Delta\tau + \mu \left(\Delta\sigma_n - B \frac{\Delta\sigma_{kk}}{3} \right). \quad (3)$$

[9] Thus, in both equations (2) and (3) the values of the friction and the Skempton coefficients have to be adopted in order to compute stress perturbations. *Cocco and Rice [2002]* discussed the difficulties in distinguishing between these two models also in realistic complex fault zones with inelastic or anisotropic properties. *Beeler et al. [2000]* suggested using equation (3) because it is more general and applicable to different tectonic areas. This represents a first source of variability in computing static coseismic stress changes, which is commonly not considered since equation (2) is widely adopted to compute seismicity rate changes [see *Beeler et al., 2000*].

2.2. Resolving Coulomb Stress Changes Onto Receiver Faults

[10] The calculation of Coulomb stress changes requires the definition of the geometry and the faulting mechanism of the target faults on which stress perturbations are resolved. Two approaches are commonly adopted; the first one relies on resolving stress changes onto a prescribed faulting mechanism (that is, to assign strike, dip, and rake angles of the target faults). This means that fault geometry and slip direction are input parameters of stress interaction simulations. *McCloskey et al. [2003]* proposed using geological constraints in order to calculate Coulomb stress perturbations for forecasting the spatial pattern of seismicity. However, this strategy does not always seem to be applicable, due to the complexity of fault systems, for instance, as pointed out by *Nothro et al. [2005]* in their application to the 1997 Umbria-Marche (Italy) seismic sequence. The second approach relies on the calculation of the optimally oriented planes (OOPs) for Coulomb failure. In this case, instead of assigning the strike, dip, and rake angles of the receiver faults, we have to assign the magnitude and the orientation of the principal axes of the regional stress field σ'_{ij} [see *King and Cocco, 2001*, and references therein]. The optimally oriented planes are identified at each grid point of the numerical computation by finding the values of strike, dip, and rake that maximize the total stress tensor defined as $\sigma'_{ij}{}^{\text{tot}} = \sigma'_{ij} + \Delta\sigma_{ij}$, where $\Delta\sigma_{ij}$ is the coseismic stress perturbation.

After assigning the absolute values of the principal stress components and the orientation of the stress tensor (trend and plunge of each axis), two equivalent OOPs are obtained at each node of the 3-D grid.

[11] The predicted focal mechanisms associated with the OOPs strongly depend on the orientation and magnitude of the regional stress field. Therefore, Coulomb stress changes computed for OOPs are associated with theoretical focal mechanisms, which might differ from real fault plane solutions. This might be the case also for stress changes resolved onto prescribed receiver faults, although in this latter case constraints from structural geology and a direct control of the expected faulting mechanisms might reduce the variability.

[12] Therefore, we remark here that resolving stress changes on receiver faults, through either the identification of prescribed receivers or the calculation of OOPs, requires assigning further input parameters. As we will discuss in the following the choice of one of these two simulation strategies will lead to completely different patterns of Coulomb stress perturbations, particularly near the causative faults.

2.3. Computing the Rate of Earthquake Production

[13] We briefly describe here the *Dieterich* [1994] model to compute the changes in the rate of earthquake production caused by coseismic stress perturbations. The seismicity rate R after the application of a stress perturbation is a function of the state variable γ , stressing rate $\dot{\tau}$ and the background seismicity rate r [see also *Toda and Stein*, 2003; *Toda et al.*, 2005]:

$$R = \frac{r}{\gamma \dot{\tau}}. \quad (4)$$

Under a constant stressing rate without stress perturbations, the state variable is at the steady state and takes the value

$$\gamma_0 = \frac{1}{\dot{\tau}}, \quad (5)$$

which according to equation (4) gives $R = r$. This implies that in the absence of any stress perturbation, the seismicity rate at the steady state is given by the background rate of earthquake production. We assume here that the stressing rate does not change before and after the main shock, being equal to $\dot{\tau}$. Following *Dieterich* [1994] the rate R can be interpreted as a statistical representation of the expected rate of earthquake production in a given magnitude range. An applied stress perturbation to the fault population modifies the seismicity rate through the evolution of the state variable given by

$$\gamma_n = \gamma_{n-1} \exp\left(\frac{-S}{A\sigma}\right), \quad (6)$$

where γ_{n-1} and γ_n are the values of the state variable just before and after the applied stress change (S), respectively. $A\sigma$ is the constitutive parameter of the rate- and state-dependent law governing fault friction; we note here that σ is the effective normal stress also named σ_{eff} in the following

of the text. The evolution of state variable is governed by the following law:

$$d\gamma = \frac{1}{A\sigma} [dt - \gamma S], \quad (7)$$

where S in equations (6) and (7) is the “modified” Coulomb stress change $S = \Delta\text{CFF}$ and is given by [*Dieterich et al.*, 2000; *Catalli et al.*, 2008, and references therein]

$$S = \Delta\text{CFF} = \Delta\tau + (\mu - \alpha)\Delta\sigma_{\text{eff}} = \Delta\tau + \mu_{\text{eff}}\Delta\sigma_{\text{eff}}, \quad (8)$$

where $\Delta\sigma_{\text{eff}} = (\Delta\sigma_n + \Delta P)$, $\mu_{\text{eff}} = (\mu - \alpha)$, where α is the positive nondimensional parameter controlling the normal stress changes in the *Linker and Dieterich* [1992] constitutive law. This parameter is necessary to account for normal stress changes in the rate- and state-dependent frictional approach, and consequently the parameter multiplying the effective normal stress changes in equation (8) is not the friction coefficient as usually assumed in Coulomb stress computations (see equation (1) and also *Harris* [1998]).

[14] A positive stress perturbation caused by an earthquake occurred nearby will decrease the state variable γ , so the target fault slips at higher rate. A drop in the state variable results in an increase in the seismicity rate. According to the *Dieterich* [1994] model, the state variable γ increases with time after the stress changes according to

$$\gamma_{n+1} = \left(\gamma_n - \frac{1}{\dot{\tau}}\right) \exp\left(\frac{-\Delta t \dot{\tau}}{A\sigma}\right) + \frac{1}{\dot{\tau}}, \quad (9)$$

where Δt is the time elapsed after the stress perturbation and γ_n is calculated through (6).

3. Impact of Model Parameters

[15] The calculation of seismicity rate changes caused by coseismic stress perturbations requires the choice of the following main input parameters: the amplitude of the Coulomb stress perturbation (which depends on other parameters as described in sections 2.1 and 2.2), the constitutive parameter $A\sigma$, the stressing rate $\dot{\tau}$, and the background seismicity rate r . In this section we focus on the last three input parameters describing the rate- and state-dependent model to forecast seismicity rate changes. *Hainzl et al.* [2009] have discussed the impact of uncertainties and variability of coseismic stress change amplitudes. We solely emphasize here that Coulomb stress changes depend on several “a priori” input parameters such as the friction and the Skempton coefficients and the α parameter of the rate and state model (see equation (8)). According to several authors [see *Harris*, 1998; *King and Cocco*, 2001; *Catalli et al.*, 2008] the effect of the friction coefficient on the stress perturbation and the seismicity rate change patterns is usually modest. On the contrary, the choice of the poroelastic model can be of relevance for computing Coulomb stress changes (equations (2) and (3)). We also point out that, according to equation (8), the effective normal stress changes are multiplied by an effective coefficient of friction that depends on both the friction coefficient and the α parameter.

3.1. Background Seismicity Rate

[16] In this section we discuss the definition of the background seismicity rate as well as its impact on the computed seismicity rate changes through the *Dieterich* [1994] model. This model assumes that before the application of a stress perturbation the state variable γ is at a steady state, which means that it does not change with time. Indeed, it is assumed that this initial value (γ_0) is equal to the inverse of the stressing rate (which is taken constant in time in the most common formulation of the Dieterich model); therefore, according to (4) the seismicity rate before the application of the stress perturbation is equal to the background rate r . We describe such a background rate through a stationary seismicity rate. The background seismicity rate r is an important variable in any fault population model. The background seismicity rate is the rate of earthquake production in absence of any stress perturbation and it is associated with a spatially nonuniform stationary process [see, e.g., *Toda et al.*, 2005]. According to this definition, background events are expected to occur independently of each other (i.e., the nucleating patches do not interact), and therefore the background seismicity rate can be also considered a time-independent Poisson process. In the present study, we refer to the “background seismicity” rate as a time-independent smoothed seismicity rate computed in a prescribed time window using a declustered catalog.

[17] Different procedures can be applied for declustering a seismic catalog. In the present study we adopt the background rate measured through the epidemic type aftershock sequence (ETAS) model [*Ogata*, 1988, 1998] following the method proposed by *Zhuang et al.* [2002]. The ETAS model defines the seismicity rate at time t and location (x, y) as the sum of two contributions

$$\lambda(t, x, y) = \mu(x, y) + \sum_{i: t_i < t} \frac{K e^{\tilde{\alpha}(M_i - M_c)}}{(t - t_i + c)^p} \frac{c_{dq}}{\left[(x - x_i)^2 + (y - y_i)^2 + d^2 \right]^q}, \quad (10)$$

where $\mu(x, y)$ is the time-independent spatially nonuniform background seismicity rate, K and $\tilde{\alpha}$ are the productivity parameters related to the numbers of events triggered by each earthquake, c is a time constant, and the exponent p controls the decay of the sequence. M_c is the completeness magnitude, while i identifies the triggering event occurring at time t_i with magnitude M_i . The variables d and q are the parameters characterizing the spatial distribution of triggered events, $\sqrt{(x - x_i)^2 + (y - y_i)^2}$ is the distance between the location (x, y) and the epicenter of the i th earthquake (x_i, y_i) and c_{dq} is a normalization factor. Therefore, using the ETAS model we can measure the spatially nonuniform (i.e., clustered in space) background seismicity rate as $r = \mu(x, y)$.

[18] The definition and the measure of a reference or a background seismicity rate is still controversial [*Hainzl and Ogata*, 2005; *Lombardi et al.*, 2006; *Lombardi and Marzocchi*, 2007] and different approaches are used in the literature. *Catalli et al.* [2008], for instance, adopted a reference seismicity rate computed by smoothing seismicity on a prescribed time window using a complete (undclustered) catalog in order to model seismicity rate changes through

the Dieterich approach. We use this definition in the present work and we refer to the “reference seismicity” rate as a time-independent smoothed seismicity rate computed by using an undclustered catalog. Thus, contrary to the background, the reference seismicity rate contains all the sequences and the triggered events within the selected time window. It is important to point out that in this latter case the reference seismicity rate cannot be considered as the rate of earthquake production in absence of any stress perturbation. To estimate in this way a stationary mean rate, the time period selected for smoothing the seismicity has to be longer than the duration of seismic sequences within the adopted time interval. The choice of the time window is relevant for both the computed background and the reference seismicity rates [*Marsan*, 2003; *Marsan and Nalbant*, 2005], but the latter is certainly more affected by this subjective choice and by the temporal variability of completeness magnitude.

[19] Figure 1 shows the calculation of the reference ($r(x, y)$, Figure 1a) and background ($\mu(x, y)$, Figure 1b) seismicity rates computed for the area struck by the 1992 Landers earthquake. The reference seismicity rate has been computed by smoothing the seismicity in the 8 years (1984–1991) preceding the 1992 main shock using the *Frankel* [1995] algorithm. The minimum magnitude used for smoothing is 3.0, the maximum depth 30 km, and the correlation distance 5 km; the adopted b value is equal to 0.91. We use in this study the same values adopted in the retrospective forecasting test described by *J. Woessner et al.* (submitted manuscript, 2009). The mean value of the reference seismicity rate is 3×10^{-6} events/d km². The background seismicity rate has been computed through equation (10) using the same minimum magnitude and time period. The mean value of the background seismicity rate is 1.5×10^{-6} events/d km². It is evident from Figure 1 that both the pattern and the absolute values of seismicity rates are different and we will show below how this difference affects the predicted seismicity rate changes.

[20] Figure 2 displays the map of the difference at each grid point between the computed reference (Figure 2, left) or background (Figure 2, right) seismicity rate and their average value measured for the whole area. This figure shows that both the background and the reference seismicity rates are larger than their associated average values in nearly the same area. As expected the variability of the reference seismicity rate is larger than that of the background rate. This figure depicts that in both cases the Big Bear aftershock lies in the area of largest positive difference between spatially nonuniform seismicity rates and their average values. On the contrary, east of the causative fault system, where the Hector Mine earthquake occurred in 1994, this difference is negative, which means that the nonuniform rates are smaller than their mean values (note that we are analyzing here the seismicity before the 1992 Landers main shock). This raises the question if a uniform background seismicity rate is a good assumption to forecast seismicity rate changes. The resulting average rates for the whole area correspond to 0.176 and 0.086 events/d for the reference and the background seismicity rate, respectively.

[21] In many studies and applications [see, e.g., *Gomberg et al.*, 2005a; *Toda and Stein*, 2003] the background seismicity rate is assumed spatially uniform. We have computed the seismicity rate changes caused by the 1992 Landers

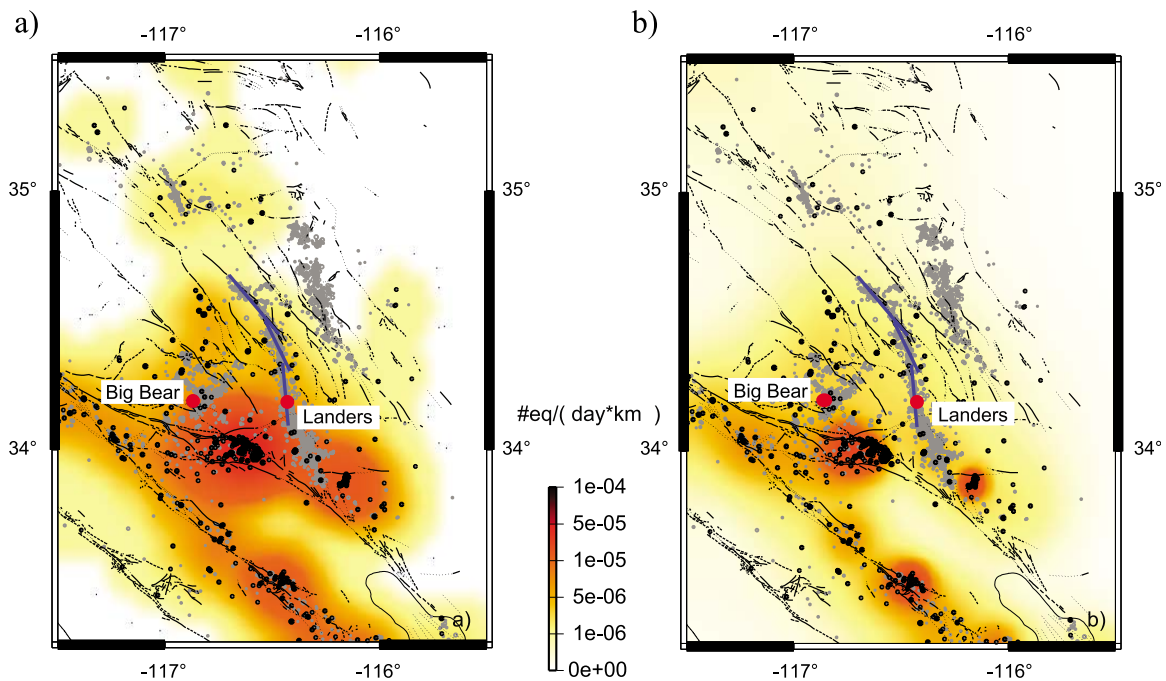


Figure 1. (a) Reference $r(x, y)$ and (b) background $\mu(x, y)$ seismicity rates computed for the study area. Red dots show the epicenter of the 1992 Landers main shock and the Big Bear aftershock. The reference seismicity rate is computed in the 8 years preceding the 1992 main shock (1984–1991) using the Frankel algorithm for smoothing the seismicity of a complete (undeclustered) catalog (see text for the details of these calculations). The background seismicity rate has been computed through equation (10) and the ETAS approach. The black dots in this figure indicate the epicenters of earthquakes occurred before the 1992 Landers main shock, while the shaded dots depicts the aftershock locations.

main shock and the Big Bear largest aftershock using the mean values of both the reference and the background seismicity rates given above. In this case, the ratio between the forecasted cumulative number of triggered earthquakes for both models (we have kept all the other parameters $A\sigma$ and $\hat{\tau}$ fixed and equal to 0.04 MPa and 5.6×10^{-6} MPa/d; these values are consistent with those proposed by *Toda et al.* [2005]) is nearly equal to the corresponding ratio between the values of the estimated background and reference seismicity rates (see Figure 3, dashed curves). A different application performed by using spatially inhomogeneous seismicity rates shows that the difference between the seismicity rate forecast performed by using $r(x, y)$ for the Landers and Big Bear shocks is significantly larger than that obtained by using the nonuniform background rate $\mu(x, y)$ (see Figure 3, solid curves) as well as those inferred by adopting the spatially uniform mean values (dashed curves). However, it is important to emphasize that this result cannot be extrapolated to other areas.

[22] We have performed similar calculations to study the 1997 Kagoshima (Japan) earthquake pair [see *Toda and Stein*, 2003]. Two strike slip earthquakes ($M \sim 6$) struck the Kagoshima prefecture (Japan) in 1997; they were just 4 km and 48 days apart and provided a good test to study stress interactions and one of the first attempts to estimate aftershock probabilities [Toda and Stein, 2003]. We have computed the background seismicity rate by applying the ETAS approach to the seismic catalog provided by the Japan

Meteorological Agency (JMA) and the reference seismicity rate by smoothing the seismicity in the 10 years preceding the first Kagoshima main shock. The minimum magnitude and the maximum depth for smoothing seismicity are 2.3 and 40 km, respectively. The adopted b value for this area is 0.9. Figure 4 shows the spatial distribution of the reference (Figure 4, left) and background (Figure 4, right) seismicity rates for the Kagoshima area, which displays evident differences. The mean value of the reference seismicity rate is 7.5×10^{-6} events/d km² and that one of the background seismicity rate is 2.5×10^{-6} events/d km². We have computed the predicted seismicity rate changes caused by the two main shocks using both the mean and the spatially variable reference and background rates. The results of the numerical simulations for Kagoshima reveal just the opposite outcome than those for Landers (see Figure 5). The seismicity rate forecast performed by using the uniform reference rate is larger than that obtained for the nonuniform reference rate and the opposite is found for forecasted seismicity rate changes inferred by using the background rates (constant and spatially nonuniform).

[23] This apparent paradox can be explained by considering that the signs of the Coulomb stress changes affect the computed cumulative number of triggered aftershocks. A high reference seismicity rate in a stress shadow area will produce no enhanced seismicity rate changes. On the contrary, a higher reference rate in a region of enhanced Coulomb stress will produce a significant increase of seismicity rate.

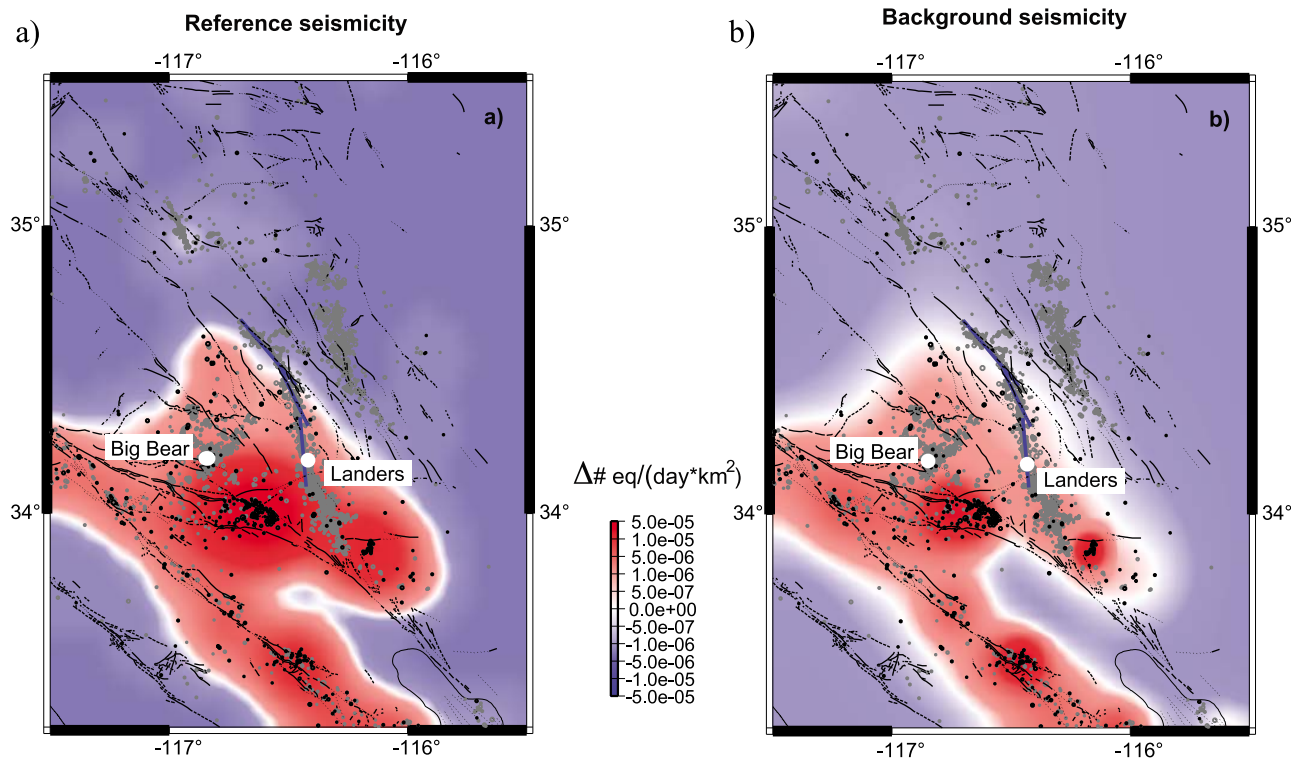


Figure 2. Difference between the spatially nonuniform seismicity rate and the average value measured for the whole area: Figure 2a displays the difference for the reference seismicity rate, while Figure 2b shows that one for the background seismicity rate. Red and blue colors indicate a local value larger or smaller than the average value, respectively.

Therefore, the expected seismicity rate change will strongly depend on the spatial correlation between applied stress changes and the background or reference seismicity rates. In particular, high seismicity rate changes are expected for positive correlations, but irrelevant changes of the rate of earthquake production for anticorrelations. Therefore, the opposite results found for the 1992 Landers and the 1997 Kagoshima earthquakes depend on the different correlation between the spatial pattern of Coulomb stress changes and seismicity rate changes.

[24] Figure 6 shows the map of Coulomb stress changes computed at 7.5 km depth (middle of the seismogenic layer) after the 1992 Landers main shock (Figure 6, left) and after the main shock and the Big Bear aftershock (Figure 6, right) using equation (2) and resolving stress changes onto prescribed target vertical faults striking 330°N (dip 90°) with a rake angle of 180° . The slip distribution for the Landers earthquake used for these calculations is taken from *Wald and Heaton* [1994], while that for the Big Bear earthquake is taken from *Jones and Hough* [1995]. The stress changes are computed for $\alpha = 0.25$, $\mu = 0.75$, and $B = 0.47$ (which yields $\mu' = 0.4$). Using these stress changes we have calculated the seismicity rate changes through equations (4), (6), and (9). A visual comparison between Figures 2 and 6 reveals that a large area with high background or reference seismicity rates lies in stress shadows.

[25] Although nonuniform background seismicity can be expected from a physical point of view, the application of inhomogeneous reference or background models should be taken with care. First, an appropriate estimation of the

spatial seismicity fluctuations requires better data coverage than is available in many applications. Second, because of the above-mentioned dependence on the spatial correlation, nonuniform background models are more sensitive to the calculated stress changes, which are known only with large uncertainties due to uncertain slip distribution, fault geometry, and small-scale stress heterogeneities (for further discussion, see *Sudhaus and Jónsson* [2009]; *Hainzl et al.* [2009]).

3.2. $A\sigma$ and the Stressing Rate

[26] The effects of individual input parameters in the Dieterich model have been previously discussed in the literature [see *Belardinelli et al.*, 1999; *Toda and Stein*, 2003; *Catalli et al.*, 2008, and references therein]. Indeed, it is well known that $A\sigma$ controls the instantaneous increase of the seismicity rate: the smaller the $A\sigma$ value the larger the seismicity rate change. Equations (6) and (7) show that this parameter controls both the instantaneous change and the following evolution of the state variable γ . *Console et al.* [2006] and *Catalli et al.* [2008] have shown that the total number of triggered events over infinite times does not depend on $A\sigma$. Indeed, the time integral of the net rate of promoted seismicity $R'(t) = R(t) - r$ over infinite times is given by

$$N_\infty = \int_0^{+\infty} R'(t) dt = \frac{r}{\tau} S. \quad (11)$$

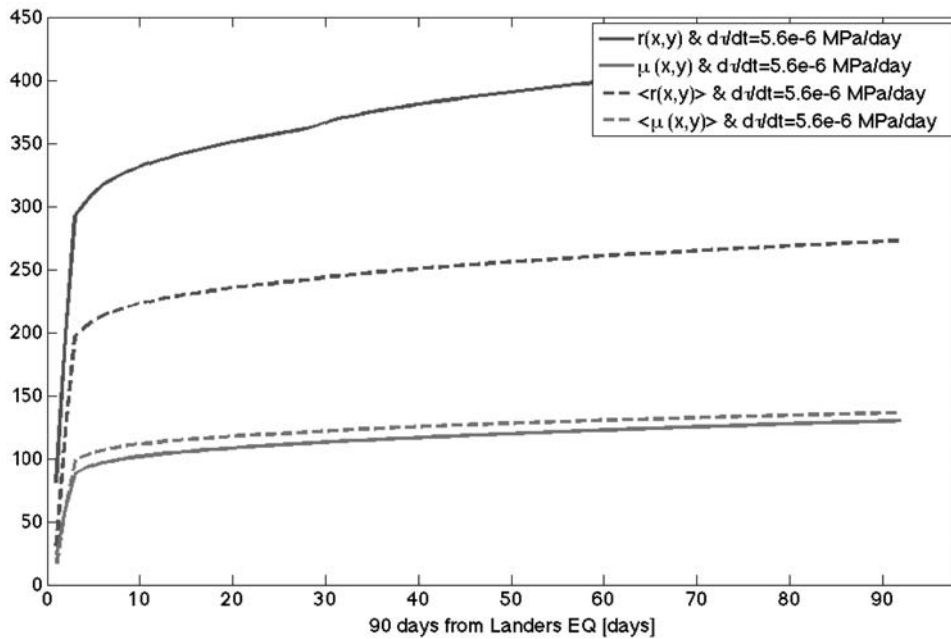


Figure 3. Cumulative number of events calculated through the *Dieterich* [1994] model assuming a spatially nonuniform reference and background seismicity rates (solid curves) and a constant reference and background seismicity rates corresponding to their average values (dashed curves). For all these calculations the stressing rate is constant $\dot{\tau} = 5.6 \times 10^{-6}$ MPa/d and $A\sigma = 0.04$ MPa. Black curves identify the calculations performed by adopting the reference seismicity rates and gray curves shows those performed by using the background seismicity rate.

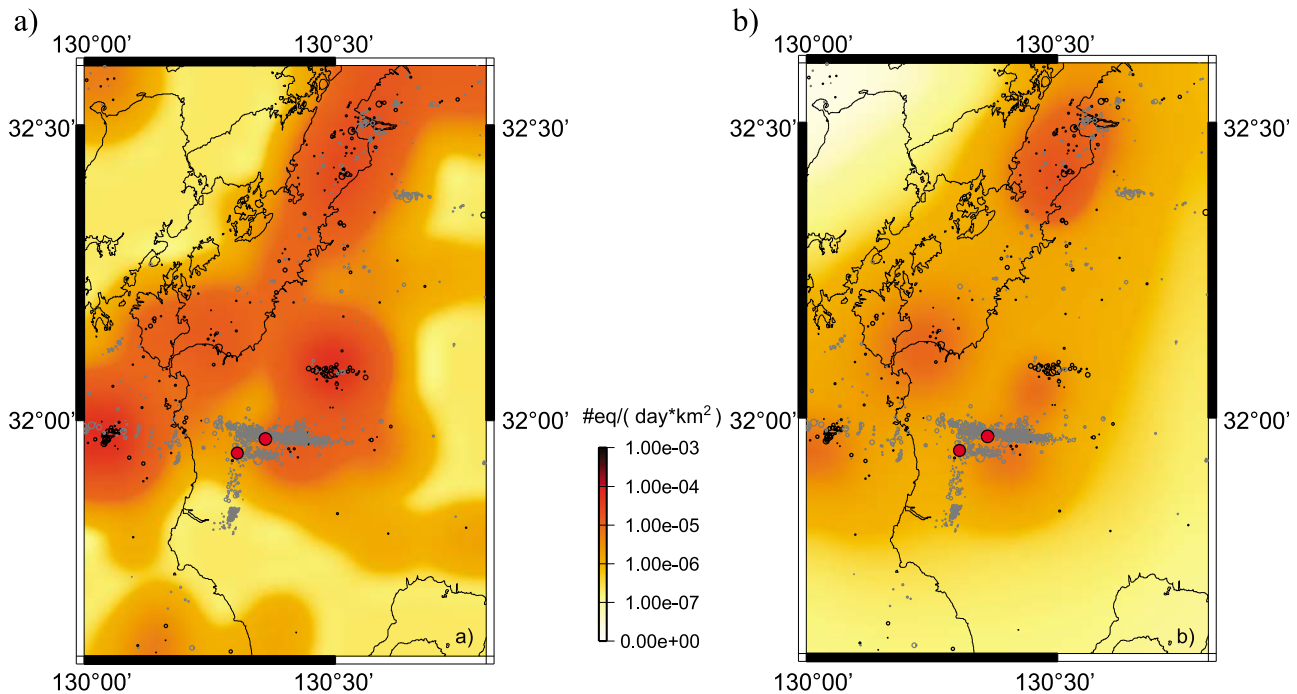


Figure 4. (a) Reference $r(x, y)$ and (b) background $\mu(x, y)$ seismicity rates computed for the 1997 Kagoshima prefecture (Japan) earthquake. The red dots show the epicenter of the two strike slip earthquakes ($M \sim 6$) occurred 48 days apart from each other. The background seismicity rate is computed by applying the ETAS approach to the seismic catalog provided by JMA, while the reference seismicity rate by smoothing the seismicity in the 10 years preceding the first Kagoshima main shock (see text for the details of these calculations). The black dots in this figure indicate the epicenters of earthquakes occurred before the first main shock, while the gray dots depicts the aftershock locations.

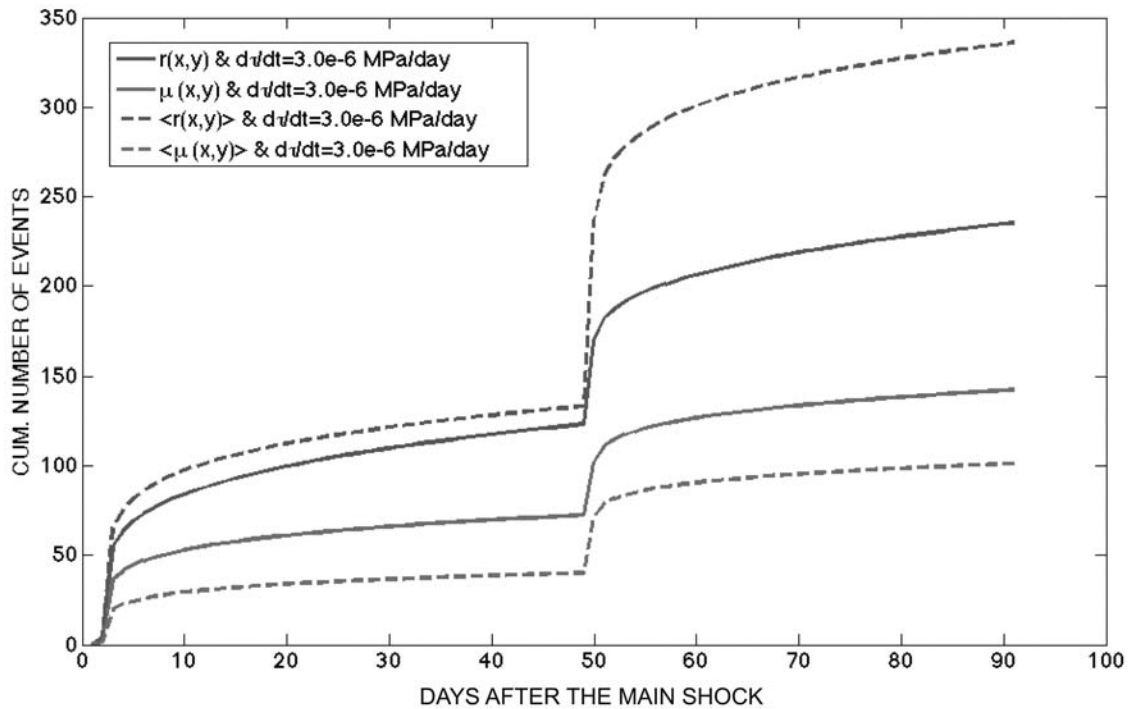


Figure 5. Cumulative number of events calculated through the *Dieterich* [1994] model assuming a spatially nonuniform reference and background seismicity rates (solid curves) and a constant reference and background seismicity rates corresponding to their average values (dashed curves) for the 1997 Kagoshima earthquake. For all these calculations the stressing rate is constant $\dot{\tau} = 3.0 \times 10^{-6}$ MPa/d and $A\sigma = 0.04$ MPa [Toda and Stein, 2003]. Black curves identify the calculations performed by adopting the reference seismicity rates and gray curves shows those performed by using the background seismicity rate.

According to this relation the net number, N_{∞} , of promoted earthquakes over infinite times depends only on the background rate, the stressing rate, and the Coulomb stress perturbation.

[27] The role of the stressing rate on the predicted seismicity rate changes has been already discussed in the literature [see Toda *et al.*, 2002; Llenos *et al.*, 2009]. It is evident from equations (5) and (9) that the stressing rate $\dot{\tau}$ controls the state variable evolution before and after the stress perturbation. The stressing rate is of particular importance for modeling the seismicity rate changes and the Omori-like aftershock decay because it controls for a given $A\sigma$ the duration of the aftershock sequence. Indeed, one of the relevant implications of the *Dieterich* [1994] approach is that the aftershock duration t_a does not depend on the magnitude of the main shock and is controlled by

$$t_a = \frac{A\sigma}{\dot{\tau}}. \quad (12)$$

[28] Thus, the rate- and state-dependent friction model for seismicity rate changes can equivalently be stated by the three parameters r , $A\sigma$, and t_a instead of r , $A\sigma$, and $\dot{\tau}$. Finally, despite equation (11) predicts that the total number of triggered events over infinite times does not depend on $A\sigma$, we emphasize that for time periods shorter than t_a , the

adopted $A\sigma$ value affects the cumulative number of triggered earthquakes.

4. Correlations Between Parameters

[29] The model parameters are strongly correlated for physical and statistical reasons. Based on the the balance of seismic moment release, *Catalli et al.* [2008] deduced an analytically approximate relation to link the stressing rate to the reference seismicity rate, under the assumption that r accounts for all the events in a given magnitude range without declustering:

$$\dot{\tau} \cong \frac{rM_0^*}{W_{\text{seis}}} \frac{b}{1.5-b} (10^{(1.5-b)(M_{\text{max}}-M^*)} - 1), \quad (13)$$

where r is the reference seismicity rate, M_0^* is the seismic moment of the magnitude M^* earthquake, W_{seis} the thickness of the seismogenic zone [Catalli *et al.*, 2008], b is the parameter of the Gutenberg-Richter distribution, and M_{max} and M^* are the maximum and minimum magnitudes, respectively. Note that in (13) the reference seismicity $r(x, y)$ must include all the earthquakes in the given magnitude range to estimate the stressing rate through the proposed approximate relation. We emphasize that this relation suggests the input parameters $\dot{\tau}$ and r of the physics-based model to be linearly correlated. According to (12) and (13) a

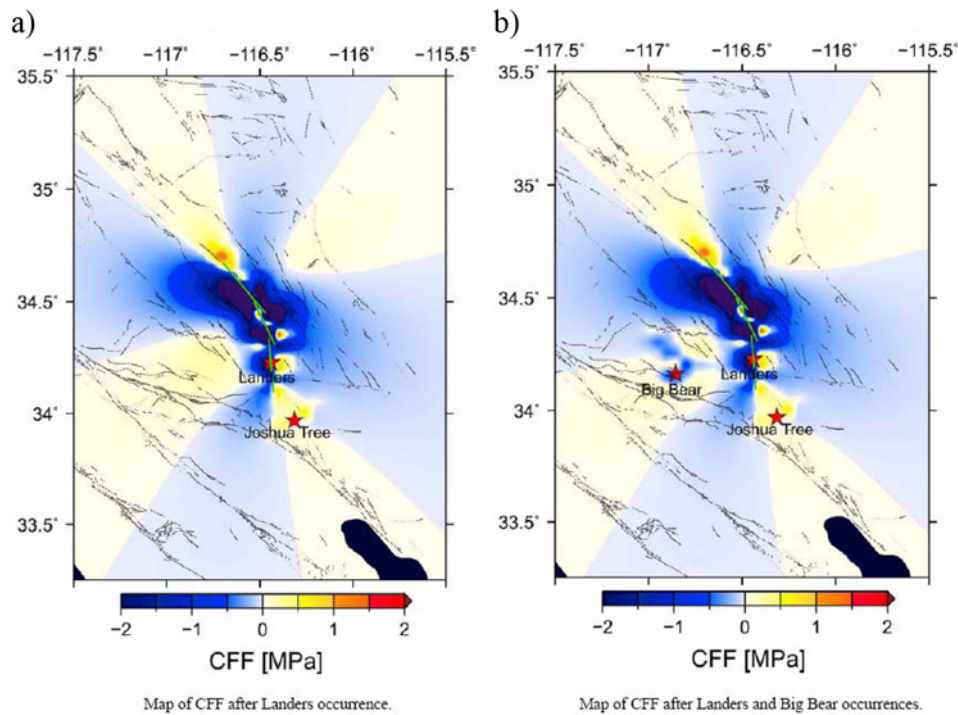


Figure 6. Static Coulomb stress changes computed at 7.5 km depth immediately after (a) the 1992 Landers main shock and (b) the Big Bear aftershock (including both the main shock and the aftershock) using the constant apparent friction model (equation (2), $\mu' = 0.4$) and resolving stress changes onto prescribed vertical strike slip faults striking 330°N (rake angle 180°). The slip distribution and the fault geometry for the 1992 Landers earthquake are taken by *Wald and Heaton* [1994], while that for the Big Bear aftershock is from *Jones and Hough* [1995].

spatially variable stressing rate (inferred from a spatially nonuniform reference seismicity rate) implies a spatially variable aftershock duration time t_a . This in turn affects the forecasted seismicity rate changes. In addition, relation (13) and equation (11) predict that the total number of triggered earthquakes over infinite times only depends on the stress change amplitude. This implies that assessing the variability of Coulomb stress changes is extremely important [*Hainzl et al.*, 2009].

[30] Even stronger correlations between the parameters are obtained from a statistical point of view if early aftershock data are available and are used to constrain input parameters for forecasting attempts. We demonstrate in the following that in the case of an observationally constrained aftershock decay, the background rate r , and the aftershock relaxation time t_a are strongly correlated to determine the aftershock productivity. This implies that according to (12) and (13) all the three main input parameters of the rate and state approach are correlated.

[31] According to the *Dieterich* [1994] model, the seismicity rate changes caused by a stress perturbation S (at time $t = 0$) can be also written in the following way, which is equivalent to (4):

$$R = \frac{r}{1 + \left[\exp\left(-\frac{S}{A\sigma}\right) - 1 \right] \exp\left(-\frac{t\dot{r}}{A\sigma}\right)}. \quad (14)$$

[32] Using relation (12) and defining $\psi = \exp\left(-\frac{S}{A\sigma}\right)$, we can write (14) as

$$R = \frac{r}{1 + (\psi - 1) \exp\left(-\frac{t}{t_a}\right)}, \quad (15)$$

which for $t \ll t_a$ becomes

$$R \approx \frac{r}{1 + (\psi - 1) \left(1 - \frac{t}{t_a}\right)} = \frac{r}{\psi - (\psi - 1) \left(\frac{t}{t_a}\right)}. \quad (16)$$

[33] After simple rearrangements (16) is written as

$$R \approx \frac{rt_a}{\left[\frac{1 - \psi}{\psi t_a} + t \right]}, \quad (17)$$

which is the Omori law with a p value equal to 1, the c value is given by

$$c = \psi t_a / (1 - \psi) \quad (18)$$

and the productivity by

$$K = r t_a / (1 - \psi). \quad (19)$$

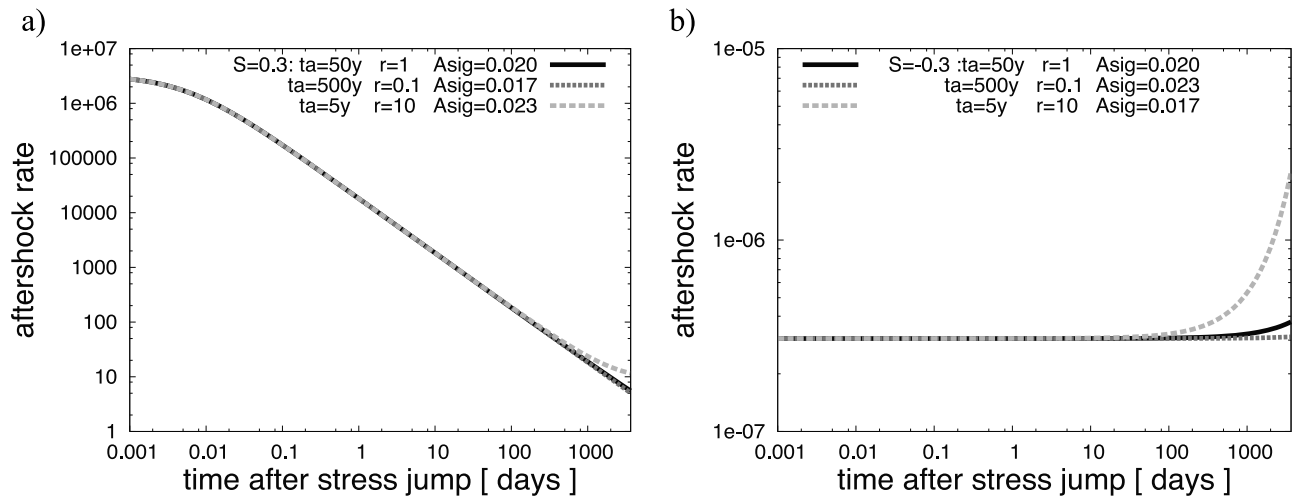


Figure 7. Rate of aftershock production in a log-log scale caused by (a) a positive and (b) a negative stress perturbations. These simulations have been performed using a stress step of 0.3 MPa. Colors indicate different combinations of the aftershock duration t_a , background rate r , and $A\sigma$ parameter. The same rate decay in the first days after the stress perturbation is obtained by different combinations of input parameters. This figure suggests an inverse correlation between background seismicity rate and aftershock duration $r \sim 1/t_a$.

These equations show that the productivity depends not only on the stressing rate [see *Llenos et al.*, 2009], but also on the background rate and the parameter $A\sigma$. However, if equation (13) holds and $\dot{\tau}$ is linearly proportional to r , $r/\dot{\tau}$ becomes constant and the productivity only depends on $A\sigma$.

[34] If the stress jump is large compared to the parameter $A\sigma$, then $1 - \psi \approx 1$ and the Omori parameters become $c \simeq \exp(-\Delta S/A\sigma) t_a$ and $K \simeq r t_a$ [see *Dieterich*, 1994]. For $c < t \ll t_a$, the rate decays according to $R \approx K/t$ and thus if the t_a is changed by a factor κ , the background rate r has to be changed by a factor $1/\kappa$ to fit the same observed decay. To get a similar fit on short time scales ($t \ll t_a$), the c value should be also the same. Our calculations imply that for a spatially uniform background rate r and tectonic loading $\dot{\tau}$, the aftershock duration t_a is also uniform but not the productivity K and the c value. The latter parameter defines the delay before the onset of the $1/t$ decay. The c parameter and the productivity depend on the ΔCFF value of the stress changes which will be spatially nonuniform and distance dependent. This implies that K and c will depend on the spatial coordinates (i.e., spatially variable) due to the spatial fluctuations of $(1 - \psi)$ around 1 and ψ above zero, respectively. The superposition of aftershock sequences with c values differing in this way has previously shown to result in apparent p values < 1 for an exponential stress distribution [*Helmstetter and Shaw*, 2006]. Smaller p values

at the beginning of aftershock sequences have been reported in several previous studies that use high-resolution waveform data to quantify early aftershocks [*Peng et al.*, 2006, 2007; *Enescu et al.*, 2007, 2009].

[35] Using the constraints from observations of the earliest aftershocks, namely the K and c value, the only free parameter that remains in (14) is t_a . Taking equations (18) and (20), we can express r and ψ as a function of the aftershock duration time t_a , $\psi = c/(c + t_a)$ and $r = K/(c + t_a)$, and we get

$$R(t) = \frac{K}{c + t_a - t_a \exp\left(-\frac{t}{t_a}\right)}, \quad (20)$$

which holds for $t < t_a$.

[36] Figure 7 summarizes the correlation between input parameters for the rate and state model. Indeed, this figure shows that, locally (i.e., for a given value of stress perturbation), almost the same decay caused by a positive or a negative stress step on short and intermediate time scales is achieved for different combinations of input parameters that follow the functional dependencies: $r t_a = \text{const.}$ and $\psi \times t_a = \text{const.}$

[37] Thus, if early aftershock observations are available to constrain the seismicity decay, the frictional parameters should not be set independently but rather in accordance with the above-mentioned relations. Aftershock forecasts

Figure 8. (a and b) Spatial distribution of predicted seismicity rate changes computed immediately after the 1992 Landers earthquake and (c and d) 30 days after the main shock. In Figures 8a and 8c, the calculations performed for prescribed receivers oriented as those used for Figure 4 are shown; in Figures 8b and 8d, those performed for OOPs associated with a horizontal σ_1 oriented 7°N , a vertical σ_2 , and a horizontal σ_3 are shown. The parameters adopted for computing Coulomb stress perturbations are those used for Figure 4. Coulomb stress perturbations are computed by averaging stress changes estimated at 7.0 km and 11 km depth. Seismicity rate changes shown in Figures 8b and 8d are caused by both the Landers main shock and the Big Bear aftershock.

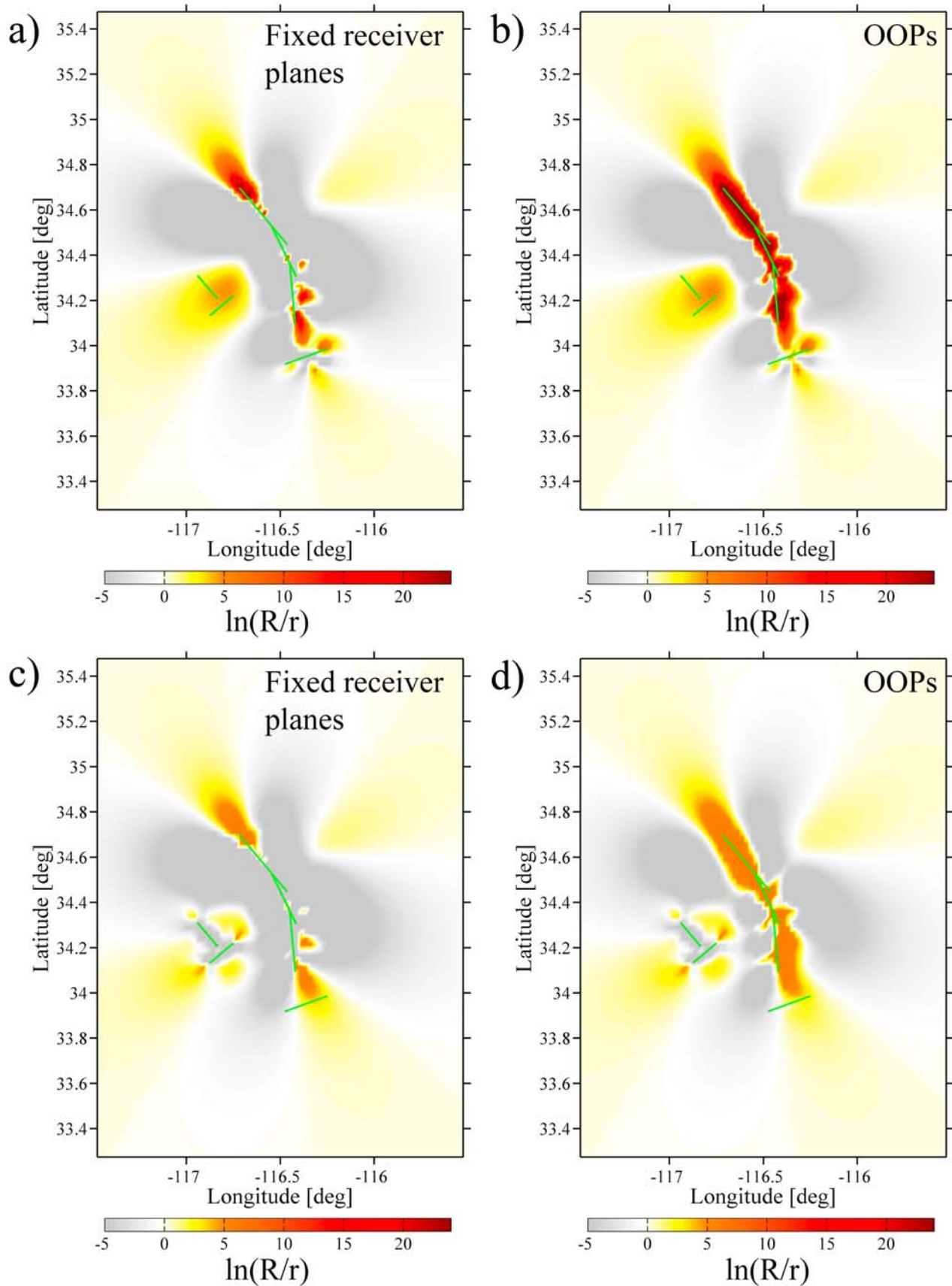


Figure 8

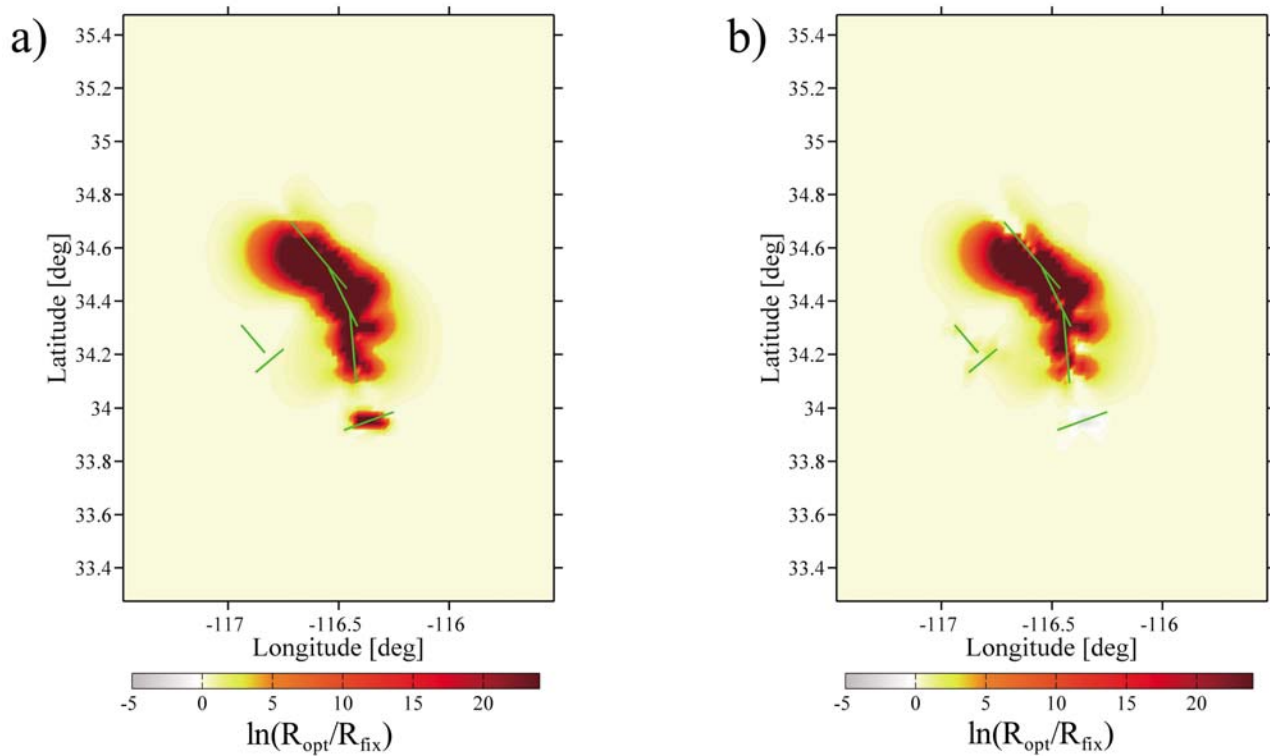


Figure 9. Spatial distribution of the difference between the seismicity rate changes computed from prescribed receivers and OOPs. (a and b) The seismicity rate difference from stress changes calculated immediately after the 1992 Landers earthquake and 30 days after the main shock, respectively.

that take these correlations implicitly into account by maximizing the likelihood function for the earliest aftershocks are discussed for the Landers case by *Hainzl et al.* [2009].

5. Forecasting Seismicity Rate Changes

[38] In this section we present as an example simulations of the rate of earthquake production caused by the 1992 Landers earthquake. We compare and discuss the model predictions based on stress changes calculated by resolving stress onto prescribed receivers as well as onto OOPs. Figure 8 displays the predicted seismicity rate changes computed from mean Coulomb stress perturbations, averaged between stress changes estimated at 7 and 11 km depth, both immediately after the main shock (Figures 8a and 8b) and 30 days after it (Figures 8c and 8d); thus, the latter includes also the stress perturbations caused by the Big Bear aftershock. The calculations are performed using the *Dieterich* [1994] model resolving stress changes onto prescribed receivers oriented as those used for Figures 4a and 4c as well as onto OOPs associated with a horizontal σ_1 oriented 7°N , a vertical σ_2 , and a horizontal σ_3 (Figures 4b and 4d). Here we have assumed the uniform background seismicity rate (0.086 events/d, corresponding to 1.5×10^{-6} events/d km²) shown in Figure 1, a constant stressing rate (2×10^{-6} MPa/d), and a value for $A\sigma$ equal to 0.02 MPa. As discussed in the previous section several combinations of these parameters can yield the same forecasts of seismicity rate if the proposed scaling is respected.

[39] Figure 9 confirms that when the only difference is resolution of stress perturbations onto prescribed receivers or OOPs, a completely different pattern of forecasted rate of earthquake production may result. This is evident close to the causative faults, where seismicity shadows predicted by the model for stress perturbations resolved onto prescribed receivers become enhanced seismicity rates for the OOPs model. In order to further point out this finding, we have shown in Figure 9 the difference between the seismicity rate changes computed for the prescribed receivers and the OOPs models. As expected the largest difference is found around the causative faults.

[40] The difference between forecasted rates of earthquake production computed adopting OOPs and prescribed receivers is evident also in the aftershock decay following the main shock. Figure 10 shows the decay rate of aftershocks predicted through mean stress changes (averaged between values estimated at 7 and 11 km depth, as in Figure 8) resolved onto OOPs (black curves) and onto prescribed receivers (gray curves). Dashed curves display the aftershock decay in areas which experienced mean stress changes smaller than 0.5 MPa, while solid curves show the whole aftershock decay for unconstrained stress perturbations. Figure 10 suggests that the difference decreases for increasing time after the main shock. The peak in the aftershock decay shown in Figure 10 is the seismicity rate change caused by the Big Bear aftershock.

[41] In some previous studies [*Toda and Stein*, 2003; *Steacy et al.*, 2004] the authors proposed excluding seismicity close to the causative faults in order to improve the

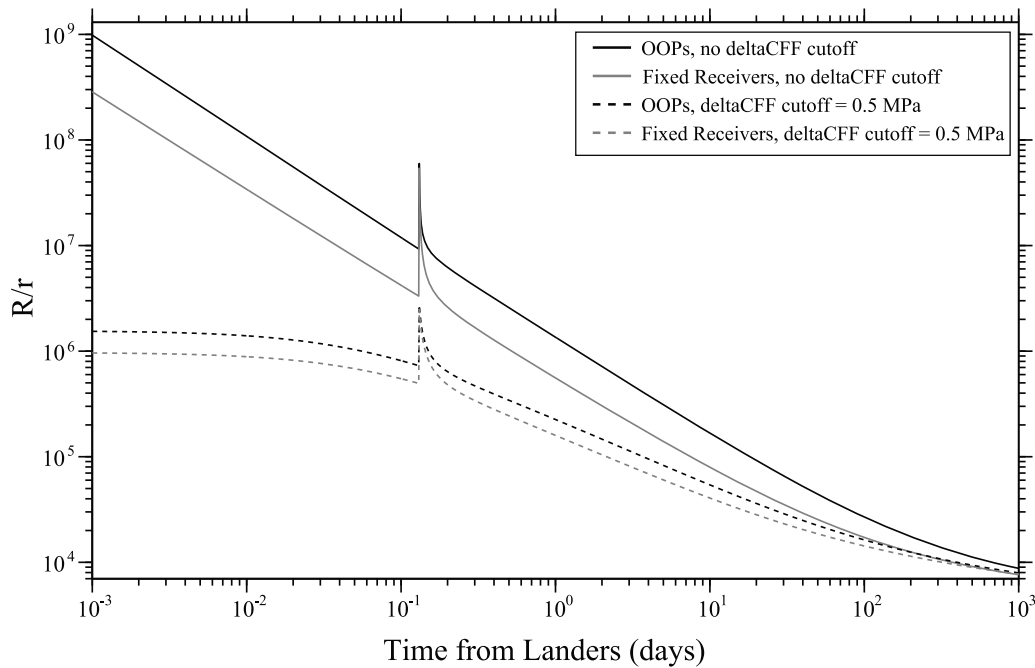


Figure 10. Temporal decay of the normalized seismicity rate changes R/r computed for OOPs (black curves) and for prescribed receivers (gray curves). Dashed lines indicate the aftershock rate decay in areas that experienced stress changes less than 0.5 MPa, while solid curves illustrate the decay rate for unrestricted stress perturbations. Input parameters for these calculations are those used for Figure 8. Seismicity rate changes are computed from mean Coulomb stress changes averaged from stress perturbations estimated at 7 and 11 km depth.

forecasted seismicity rate changes. Figure 10 shows the consequences of limiting the computed Coulomb stress changes, which indirectly corresponds to excluding near-fault regions. This figure suggests that the choice of this simulation strategy has important implications on the predicted temporal decay of early aftershocks.

6. Discussion and Concluding Remarks

[42] The application of physics-based models to near-real-time forecast attempts requires a robust validation through retrospective modeling and statistical tests. In order to perform these applications the input model parameters have to be constrained a priori based on the available data and information for the target study area. Previous studies constrain model parameters with different strategies and sometimes without a comprehensive analysis of their correlation. In this study we aim to understand the impact of physical model parameters in forecasting seismicity rate changes.

[43] We use the *Dieterich* [1994] model which is widely used to simulate the changes in the rate of earthquake production caused by stress changes. In this study we focus on the main input parameters of the *Dieterich*'s approach: the physical constitutive properties of faults (represented by the parameter $A\sigma$), the stressing rate and the reference seismicity rate of the study area. *Hainzl et al.* [2009] have discussed the effect of the variability of the amplitude of stress perturbations as well as the effect of small-scale heterogeneities characterizing the stress change pattern near

the causative faults [see also *Marsan, 2006; Helmstetter and Shaw, 2006*].

[44] A number of input parameters have to be constrained to compute stress perturbations and the associated seismicity rate changes. These model parameters are strongly correlated. Our inferred correlations demonstrate that different sets of model parameters can yield the same rate of aftershock decay. In particular, the rate- and state-dependent friction model for seismicity rate changes can equivalently be formulated in terms of the three parameters r , $A\sigma$, and $\dot{\tau}$, as well as r , A , and t_a . One relevant implication is that the inferred correlations do not allow the physical interpretation of adopted values of model parameters. In other words, it is difficult to compare values of $A\sigma$ parameter inferred from modeling the rate of earthquake production with those resulting from laboratory experiments of rock friction. At the same time, it is difficult to constrain $A\sigma$ from the aftershock decay parameter t_a , as commonly done in the literature, because this estimate depends on the correlation with the stressing rate $\dot{\tau}$.

[45] An important choice is the definition of the background seismicity rate, in particular, the use of declustered or nondeclustered precursory seismicity and its spatial variability. Despite the use of spatially variable reference or background seismicity rates is physically reasonable and corroborated by observations [see, e.g., *Toda and Stein, 2003; Zhuang et al., 2002; Toda et al., 2005*], the application of these models is not straightforward because of the spatial correlation between seismicity rate and the pattern of calculated stress perturbations. Indeed, spatially nonuniform background models are more sensitive to the uncertainties of

slip distribution as well as to the heterogeneity of stress patterns. This can discourage the adoption of nonuniform reference or background seismicity rates to forecast the rate of earthquake production.

[46] Assuming a constant background seismicity rate has also implications on the stressing rate. *Catalli et al.* [2008] have used spatially variable stressing rate patterns inferred from nonuniform reference seismicity rates through relation (13). However, this choice implies: (1) a dependence on the maximum magnitude for the study area, (2) a spatially variable t_a , (3) the lack of a depth dependence (since $\dot{\tau}$ is computed from seismicity in the whole seismogenic layer), and, finally, (4) a correlation between two of three input parameters of the Dieterich model (r and $\dot{\tau}$ or t_a). For these reasons, a constant stressing rate seems to be preferable together with a spatially uniform reference seismicity rate. These considerations also suggest to conclude that using the background seismicity rate instead of the reference rate is a more effective assumption to forecast the rate of earthquake production. This will also guarantee better satisfaction of the assumption of a stationary seismicity rate before the application of the stress perturbation.

[47] *Llenos et al.* [2009] discuss the effect of temporal changes of stressing rate caused by aseismic deformation and their effect to the background and the aftershock rates. In agreement with these authors, we have shown in this study that the aftershock productivity depends on the stressing rate [see equations (17) and (20)]. *Llenos et al.* [2009] analyzed the rate of earthquake production during several seismic swarms and concluded that the stressing rate transients increase the background seismicity rate without affecting the clustered (i.e., triggered) seismicity rate. This contradicts the predictions of the *Dieterich* [1994] model, when background seismicity and stressing rates are assumed to be uncorrelated (as in numerous applications published in the literature). In the present study, we investigate the rate of earthquake production following a large earthquake. We assume that the stressing rate does not change before and after the application of the stress perturbation. This also allows the use of Coulomb stress changes (instead of shear stress perturbations) to model the evolution of the gamma variable. Our results suggest that for aftershock sequences the productivity depends on both the background seismicity and the stressing rates [see equation (17)] and that, because of the correlation between model parameters, it is impossible to separate their contributions by analyzing aftershock decay rates in real sequences.

[48] The analysis of correlations among model parameters discussed in this study (equations (16) and (17)) relies on the assumption that $t \ll t_a$. The inferred correlations are relevant for near-real time (i.e., short term) forecast attempts. Indeed, we have shown that these correlations hold at short time scales. However, the definition of “short” time scale depends on t_a . It has to be noted, however, that the predicted aftershock decay for longer times (that is, when $t \ll t_a$ does not hold) might deviate from the expected Omori law.

[49] Finally, we emphasize that two alternative modeling strategies to resolve Coulomb stress changes on target receivers (OOPs or prescribed receivers), which are both likely choices for near-real-time applications, yield very different predictions of seismicity rate changes [see *Stacey et al.*, 2005b]. In particular, these authors and *Hainzl et al.*

[2009] concluded that models that incorporate the regional stress field (i.e., OOPs) tend to produce stress maps that best fit the observed spatial aftershock distribution. We emphasize, however, that the improved ability to forecast seismicity rate changes may be achieved renouncing to match the aftershock focal mechanisms. We also point out here that the expected variations in modeled Coulomb stress changes through equations (2) and (3) represent a further contribution to the uncertainties in stress perturbation amplitudes. This further suggests the need to include uncertainties and variability of stress amplitudes in forecasting seismicity rate changes.

[50] The results of the present study are of relevance to (i) identify reliable strategies for constraining model parameters for forecasting attempts, (ii) interpret the result of the retrospective statistical tests (see *J. Woessner et al.*, submitted manuscript, 2009), (iii) emphasize the necessity of reducing the “a priori” choices to compute Coulomb stress perturbations.

[51] Most of applications constrain model parameters from seismicity before the origin time of the causative main shock, thus analyzing the background seismicity rate. However, the results of this study suggest that early aftershocks, when available, can also be used to constrain model parameters. This can be done, for instance, by computing background stationary seismicity rate through the ETAS approach. This strategy is novel and original and relies on the acknowledgment that model parameters have to be constrained taking into account their correlations and the scaling relations proposed in this study.

[52] **Acknowledgments.** We thank S. Wiemer and W. Marzocchi for useful discussions and criticisms. We thank the SAFER-WP5 team for an effective cooperation and fruitful discussions. This work is part of the EU project SAFER, contract 036935. We have benefitted from interactions and collaborations with the research unit JRA2 of the NERIES EU project, contract 026130.

References

- Beeler, N. M., R. W. Simpson, S. H. Hickman, and D. A. Lockner (2000), Pore fluid pressure, apparent friction, and Coulomb failure, *J. Geophys. Res.*, *105*(B11), 25,533–25,542.
- Belardinelli, M. E., M. Cocco, O. Coutant, and F. Cotton (1999), Redistribution of dynamic stress during coseismic ruptures: Evidence for fault interaction and earthquake triggering, *J. Geophys. Res.*, *104*(B7), 14,925–14,945.
- Catalli, F., M. Cocco, R. Console, and L. Chiaraluce (2008), Modeling seismicity rate changes during the 1997 Umbria-Marche sequence (central Italy) through rate- and state-dependent model, *J. Geophys. Res.*, *113*, B11301, doi:10.1029/2007JB005356.
- Cocco, M., and J. R. Rice (2002), Pore pressure and poroelasticity effects in Coulomb stress analysis of earthquake interactions, *J. Geophys. Res.*, *107*(B2), 2030, doi:10.1029/2000JB000138.
- Console, R., M. Murru, and F. Catalli (2006), Physical and stochastic models of earthquake clustering, *Tectonophysics*, *417*(1–2), 141–153.
- Dieterich, J. H. (1992), Earthquake nucleation on faults with rate- and state-dependent friction, *Tectonophysics*, *211*, 115–134.
- Dieterich, J. H. (1994), A constitutive law for rate of earthquake production and its application to earthquake clustering, *J. Geophys. Res.*, *99*(B2), 2601–2618.
- Dieterich, J. H., V. Cayol, and P. Okubo (2000), The use of earthquake rate changes as a stress meter at Kilauea volcano, *Nature*, *408*, 457–460.
- Enescu, B., J. Mori, and M. Miyazawa (2007), Quantifying early aftershock activity of the 2004 mid-Niigata Prefecture earthquake, *J. Geophys. Res.*, *112*, B04310, doi:10.1029/2006JB004629.
- Enescu, B., J. Mori, M. Miyazawa, and Y. Kano (2009), Omori-Utsu Law c -values Associated with Recent Moderate Earthquakes in Japan, *Bull. Seismol. Soc. Am.*, *99*(2A), 884–891, doi:10.1785/0120080211.

- Frankel, A. (1995), Mapping seismic hazard in the central and eastern United States, *Seismol. Res. Lett.*, *66*, 8–21.
- Freed, A. M. (2005), Earthquake triggering by static, dynamic, and post-seismic stress transfer, *Annu. Rev. Earth Planet. Sci.*, *33*, 335–367.
- Gomberg, J., P. Reasenberg, M. Cocco, and M. E. Belardinelli (2005a), A frictional population model of seismicity rate change, *J. Geophys. Res.*, *110*(B5), B05S03, doi:10.1029/2004JB003404.
- Gomberg, J., M. E. Belardinelli, M. Cocco, and P. A. Reasenberg (2005b), Time-dependent earthquake probabilities, *J. Geophys. Res.*, *110*, B05S04, doi:10.1029/2004JB003405.
- Gross, S. (2001), A model of tectonic stress state and rate using the 1994 Northridge earthquake sequence, *Bull. Seismol. Soc. Am.*, *91*(2), 263–275.
- Hainzl, S., and Y. Ogata (2005), Detecting fluid signals in seismicity data through statistical earthquake modeling, *J. Geophys. Res.*, *110*, B05S07, doi:10.1029/2004JB003247.
- Hainzl, S., B. Enescu, M. Cocco, J. Woessner, C. Catalli, R. Wang, and F. Roth (2009), Aftershock modeling based on uncertain stress calculations, *J. Geophys. Res.*, *114*, B05309, doi:10.1029/2008JB006011.
- Hardebeck, J. L. (2004), Stress triggering and earthquake probability estimates, *J. Geophys. Res.*, *109*, B04310, doi:10.1029/2003JB002437.
- Harris, R. A. (1998), Introduction to special section: Stress triggers, stress shadows, and implications for seismic hazard, *J. Geophys. Res.*, *103*(B10), 24,347–24,358.
- Helmstetter, A., and B. E. Shaw (2006), Relation between stress heterogeneity and aftershock rate in the rate-and-state model, *J. Geophys. Res.*, *111*, B07304, doi:10.1029/2005JB004077.
- Jones, L. E., and S. E. Hough (1995), Analysis of broadband records from the 28 June 1992 Big Bear earthquake: Evidence of a multiple-event source, *Bull. Seismol. Soc. Am.*, *85*(3), 688–704.
- King, G. C. P., and M. Cocco (2001), Fault interaction by elastic stress changes: New clues from earthquake sequences, *Adv. Geophys.*, *44*, 1–38.
- Linker, M. F., and J. H. Dieterich (1992), Effects of variable normal stress on rock friction: Observations and constitutive equations, *J. Geophys. Res.*, *97*(B4), 4923–4940.
- Llenos, A. L., J. J. McGuire, and Y. Ogata (2009), Modeling seismic swarms triggered by aseismic transients, *J. Earth Planet. Sci. Lett.*, *281*, 59–69.
- Lombardi, A. M., and W. Marzocchi (2007), Evidence of clustering and nonstationarity in the time distribution of large worldwide earthquakes, *J. Geophys. Res.*, *112*, B02303, doi:10.1029/2006JB004568.
- Lombardi, A. M., W. Marzocchi, and J. Selva (2006), Exploring the evolution of a volcanic seismic swarm: The case of the 2000 Izu Islands swarm, *Geophys. Res. Lett.*, *33*, L07310, doi:10.1029/2005GL025157.
- Marsan, D. (2003), Triggering of seismicity at short timescales following Californian earthquakes, *J. Geophys. Res.*, *108*(B5), 2266, doi:10.1029/2002JB001946.
- Marsan, D. (2006), Can coseismic stress variability suppress seismicity shadows? Insights from a rate-and-state friction model, *J. Geophys. Res.*, *111*, B06305, doi:10.1029/2005JB004060.
- Marsan, D., and S. S. Nalbant (2005), Methods for measuring seismicity rate changes: A review and a study of how the M-w 7.3 Landers earthquake affected the aftershock sequence of the M-w 6.1 Joshua Tree earthquake, *Pure Appl. Geophys.*, *162*(6–7), 1151–1185.
- McCloskey, J., S. S. Nalbant, S. Steacy, C. Nostro, O. Scotti, and D. Baumont (2003), Structural constraints on the spatial distribution of aftershocks, *Geophys. Res. Lett.*, *30*(12), 1610, doi:10.1029/2003GL017225.
- Nostro, C., L. Chiaraluce, M. Cocco, D. Baumont, and O. Scotti (2005), Coulomb stress changes caused by repeated normal faulting earthquakes during the 1997 Umbria-Marche (central Italy) seismic sequence, *J. Geophys. Res.*, *110*, B05S20, doi:10.1029/2004JB003386.
- Ogata, Y. (1988), Statistical models of point occurrences and residual analysis for point processes, *J. Am. Stat. Assoc.*, *83*, 9–27.
- Ogata, Y. (1998), Space-time point-process models for earthquake occurrences, *Ann. Inst. Statist. Math.*, *50*, 379–402.
- Parsons, T., S. Toda, R. S. Stein, A. Barka, and J. H. Dieterich (2000), Heightened odds of large earthquakes near Istanbul: An interaction-based probability calculation, *Science*, *288*, 661–665.
- Peng, Z., J. E. Vidale, and H. Houston (2006), Anomalous early aftershock decay rate of the 2004 M_w 6.0 Parkfield, California, earthquake, *Geophys. Res. Lett.*, *33*, L17307, doi:10.1029/2006GL026744.
- Peng, Z., J. E. Vidale, M. Ishii, and A. Helmstetter (2007), Seismicity rate immediately before and after main shock rupture from high-frequency waveforms in Japan, *J. Geophys. Res.*, *112*, B03306, doi:10.1029/2006JB004386.
- Steacy, S., D. Marsan, S. S. Nalbant, and J. McCloskey (2004), Sensitivity of static stress calculations to the earthquake slip distribution, *J. Geophys. Res.*, *109*, B04303, doi:10.1029/2002JB002365.
- Steacy, S., J. Gomberg, and M. Cocco (2005a), Introduction to special section: Stress transfer, earthquake triggering, and time-dependent seismic hazard, *J. Geophys. Res.*, *110*(B5), B05S01, doi:10.1029/2005JB003692.
- Steacy, S., S. S. Nalbant, J. McCloskey, C. Nostro, O. Scotti, and D. Baumont (2005b), Onto what planes should Coulomb stress perturbations be resolved?, *J. Geophys. Res.*, *110*(B5), B05S15, doi:10.1029/2004JB003356.
- Stein, R. S. (1999), The role of stress transfer in earthquake occurrence, *Nature*, *402*(6762), 605–609.
- Stein, R. S., A. A. Barka, and J. H. Dieterich (1997), Progressive failure on the North Anatolian fault since 1939 by earthquake stress triggering, *Geophys. J. Int.*, *128*(3), 594–604.
- Sudhaus, H., and S. Jónsson (2009), Improved source modelling through combined use of InSAR and GPS under consideration of correlated data errors: application to the June 2000 Kleifarvatn earthquake, Iceland, *Geophys. J. Int.*, *176*(2), 389–404, doi: 10.1111/j.1365-246X.2008.03989.x.
- Toda, S., and R. Stein (2003), Toggling of seismicity by the 1997 Kagoshima earthquake couplet: A demonstration of time-dependent stress transfer, *J. Geophys. Res.*, *108*(B12), 2567, doi:10.1029/2003JB002527.
- Toda, S., R. S. Stein, P. A. Reasenberg, J. H. Dieterich, and A. Yoshida (1998), Stress transferred by the 1995, M_w = 6.9 Kobe, Japan, shock: Effect on aftershocks and future earthquake probabilities, *J. Geophys. Res.*, *103*(B10), 24,543–24,565.
- Toda, S., R. S. Stein, and S. Takeshi (2002), Evidence from the AD 2000 Izu Islands earthquake swarm that stressing rate governs seismicity, *Nature*, *419*, 58–61.
- Toda, S., R. S. Stein, K. Richards-Dinger, and S. B. Bozkurt (2005), Forecasting the evolution of seismicity in southern California: Animations built on earthquake stress transfer, *J. Geophys. Res.*, *110*(B5), B05S16, doi:10.1029/2004JB003415.
- Wald, D. J., and T. H. Heaton (1994), Spatial and temporal distribution of slip for the 1992 Landers, California, Earthquake, *Bull. Seismol. Soc. Am.*, *84*(3), 668–691.
- Zhuang, J., Y. Ogata, and D. Vere-Jones (2002), Stochastic declustering of space-time earthquake occurrences, *J. Am. Stat. Assoc.*, *97*, 369–380.

F. Catalli, M. Cocco, and A. M. Lombardi, INGV Rome, Istituto Nazionale di Geofisica e Vulcanologia, Sezione Seismologia e Tettonofisica, Via di Vigna Murata 605, I-00143 Rome, Italy. (cocco@ingv.it)

B. Enescu and S. Hainzl, Helmholtz Centre Potsdam, GFZ German Research Centre for Geosciences, D-14473 Potsdam, Germany.

J. Woessner, Swiss Seismological Service, ETH Zurich, CH-8092 Zurich, Switzerland.